Simultaneous Influence of Imperfect Length and Load on the Dynamic Buckling of Plane Trusses under Step Loading

Tran Thi Thuy Van
Hanoi Architectural University, Vietnam
vanttt@hau.edu.vn

Dao Ngoc Tien
Hanoi Architectural University, Vietnam
tiendn@hau.edu.vn

Ta Duy Hien
University of Transport and Communications, Vietnam
tdhien@utc.edu.vn (corresponding author)

Received: 24 April 2024 | Revised: 14 May 2024 | Accepted: 17 May 2024

 DOI: https://doi.org/10.48084/etasr.7626

ABSTRACT

The influence of imperfections in element length and loading on the dynamic buckling of plane trusses is investigated in the present study. Finite element formulation and the Euler formula are employed to tackle the problem of large displacements. Equivalently, the Newmark integration method and the Newton–Raphson iteration algorithm are deployed to solve the nonlinear dynamic equilibrium equations. The dynamic applied load considered in this study is a step-imperfect load with an imperfection in the element length. The relationship between the load and maximum displacement is determined, and the simultaneous influence of the imperfect parameters on the dynamic limit load is discussed. The imperfect element length and loading significantly affect the dynamic limit load, demonstrating the need to consider both imperfections when studying the dynamic buckling of truss systems.

Keywords-dynamic buckling; dynamic stability; dynamic limit load; dynamic response; length imperfection; loading imperfection; nonlinear analysis

I. INTRODUCTION

The vibration and buckling of beams, frames, plates, and trusses have been topics of significant interest for several years [1-8]. Authors in [8] proposed an approach to the problem of dynamic buckling in trusses based on the hybrid Finite Element Method (FEM). This method considers the influence of imperfections by setting the imperfect length as a parameter in the stiffness matrix. The results demonstrated that imperfections significantly affect the dynamic response and dynamic limit load of the truss. However, the imperfections in the element length and loading were considered independently, which is an issue that needs to be addressed.

The current study suggests a modification to the nonlinear dynamic equilibrium equations used in [8] to simultaneously account for both the imperfect load and element length parameters. The buckling of trusses under static loading has been extensively studied [9-19], nevertheless, the number of reports on dynamic buckling of trusses is relatively limited, while the imperfection factor has not been considered [19-25]. Authors in [22] investigated the buckling of truss systems under different dynamic loads. The analysis procedure was based on the FEM, considering the large displacements of the truss nodes and assuming linear elastic material behavior. All elements were alleged to be geometrically perfect, neglecting the local buckling effects of the truss elements and damping reduction. Authors in [23] examined the dynamic buckling of trusses under the same three types of loads discussed in [22]. In addition, to account for large displacements, as in [22], nonlinear material behavior was considered and the truss elements were presumed to be geometrically perfect. The results disclosed that in the case of the truss under step loading, the value of the limit load is lower than that obtained from the static analysis.

Based on the vector form the intrinsic FEM, authors in [24] proposed a method for nonlinear analysis of dynamic loading in trusses. This method can simulate significant geometric changes during the motion of a truss without utilizing

geometric stiffness matrices or iterations. The truss in [24] is also considered to be composed of geometrically perfect linear elastic elements, neglecting the local buckling effects of truss elements and damping reduction. The results were consistent with those in [22, 23], but were obtained following a simpler computational process. In [26], the Newmark Integration Method and the Newton–Raphson iteration algorithm were applied to solve nonlinear dynamic equilibrium equations. The limit load was determined according to the criteria of Budiansky–Roth. The load-maximum displacement relationship was presented for two truss types: the von Mises truss and the 01-layer roof truss. Specifically, step loading was investigated, while considering the imperfect factor. The curve of the load-maximum displacement was identified, and the simultaneous influence of the two imperfection factors on the value of the dynamic limit load was analyzed. The findings indicated that the concurrent influence of the two imperfection factors essentially affected the dynamic limit load. This underscores the necessity of synchronously considering the imperfect length and load factors when studying the dynamic buckling of trusses.

II. DYNAMIC EQUILIBRIUM OF TRUSS ELEMENTS AND SYSTEMS

A. Dynamic Equilibrium of Truss Elements

The structural elements of the truss, as illustrated in Figure 1, consist of perfect and imperfect member lengths. The symbols described as: $\{X_1, Y_1\}$, $\{X_2, Y_2\}$ are nodal coordinates of the $\{i^{th}, j^{th}\}$ elements before deformation, L_e is the initial length imperfection in length parameter Δ_e, while L_0 and L represent the distances between two nodes before and after deformation, respectively. E is the elastic modulus, A is the cross-sectional area, $f_{1.2.3.4}$ denote the nodal forces, $u_{1.2.3.4}$ denote the nodal displacements, m is the nodal mass, f_I is the inertial force, f_D is the damping force, $P(t)$ is the applied load, N is the axial force, and $u_5 = f_e = N$ represents the unknown axial force. The Euler coordinate system (x, y) is attached to the elements throughout the motion. The element length after deformation is a function of displacement [8]:

$$L = \sqrt{(X_2 - X_1 + u_3 - u_1)^2 + (Y_2 - Y_1 + u_4 - u_2)^2} \quad (1)$$

The deformations of the members are expressed by:

$$\varepsilon_x^{(e_I)} = \frac{\Delta L^{(e_I)}}{L_0}, \quad \varepsilon_x^{(e_{II})} = \frac{\Delta L^{(e_{II})}}{L_e} \quad (2)$$

where:

$$\Delta L^{(e_I)} = L - \sqrt{(X_2 - X_1)^2 + (Y_2 - Y_1)^2},$$

$$\Delta L^{(e_{II})} = L - \sqrt{(X_2 - X_1)^2 + (Y_2 - Y_1)^2} + \Delta_e$$

Applying the virtual principle, the relationship between the internal force $\boldsymbol{q}_e(\boldsymbol{u}, \Delta_e)$ and the nodal external force $\boldsymbol{f}$ can be derived:

$$\boldsymbol{q}_e(\boldsymbol{u}, \Delta_e) = \boldsymbol{f}_e \quad (3)$$

where the internal force is:

$$\boldsymbol{q}_e(\mathbf{u}, \Delta_e) = \frac{EA}{L_e}(L - L_0 + \Delta_e)\frac{\partial L}{\partial \boldsymbol{u}}$$

The nodal external force equals to the sum of the inertial force, the damping force, and the applied load [8]:

$$\boldsymbol{f}_e = \boldsymbol{f}_{I,e} + \boldsymbol{f}_{D,e} + \boldsymbol{P}_e = -\boldsymbol{m}.\ddot{\boldsymbol{u}} - \boldsymbol{c}.\ddot{\boldsymbol{u}} + \boldsymbol{P}_e . \quad (4)$$

From (3) and (4), the dynamic equilibrium equation and incremental equilibrium equation of the truss element can be obtained [8]:

$$\begin{aligned} &\boldsymbol{m}.\ddot{\boldsymbol{u}} + \boldsymbol{c}.\dot{\boldsymbol{u}} + \boldsymbol{q}_e(\boldsymbol{u}, \Delta_e) = \boldsymbol{P}_e \\ &\boldsymbol{m}.\delta\ddot{\boldsymbol{u}} + \boldsymbol{c}.\delta\dot{\boldsymbol{u}} + \boldsymbol{k}_e(\boldsymbol{u}, \Delta_e)\delta\boldsymbol{u} = \Delta\boldsymbol{P}_e \end{aligned} \quad (5)$$

where $\boldsymbol{k}_e(\boldsymbol{u}, \Delta_e) = \frac{\partial \boldsymbol{q}_e(\boldsymbol{u}, \Delta_e)}{\partial \boldsymbol{u}}$ is the tangent stiffness matrix of the truss element. Specific details regarding the stiffness matrix can be detected in [8].

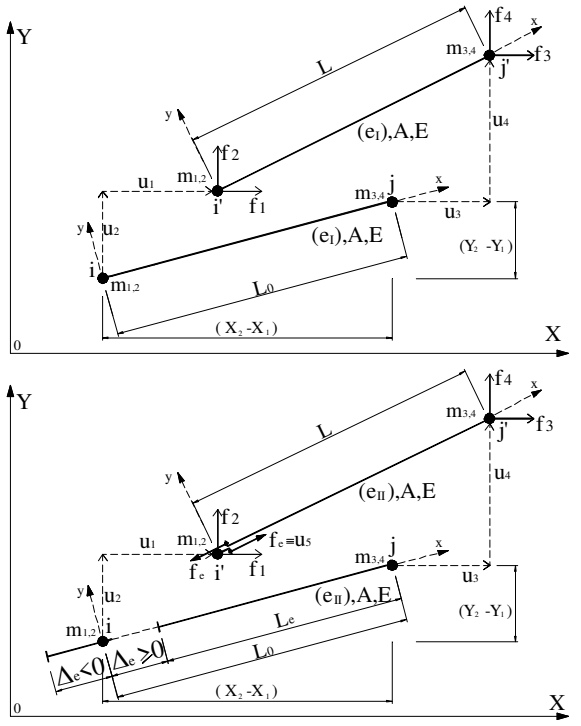

Fig. 1. Perfect (e_I) and imperfect (e_{II}) truss element models.

To simultaneously consider the case of imperfect loads with imperfect element lengths, this study proposes a modification of (5), which becomes (6) by adding an imperfect load vector to its right side:

$$\begin{aligned} &\boldsymbol{m}.\ddot{\boldsymbol{u}} + \boldsymbol{c}.\dot{\boldsymbol{u}} + \boldsymbol{q}_e(\boldsymbol{u}, \Delta_e) = \boldsymbol{P}_e + \boldsymbol{P}_{e,(imperfect)} \\ &\boldsymbol{m}.\delta\ddot{\boldsymbol{u}} + \boldsymbol{c}.\delta\dot{\boldsymbol{u}} + \boldsymbol{k}_e(\boldsymbol{u}, \Delta_e)\delta\boldsymbol{u} = \Delta\boldsymbol{P}_e + \Delta\boldsymbol{P}_{e,(imperfect)} \end{aligned} \quad (6)$$

In (6), the left-hand side contains the parameter of imperfect length Δ_e, whereas the right side contains the parameter of imperfect load $\Delta \boldsymbol{P}_{imperfect}$.

B. Dynamic Equilibrium of the Truss System

The equilibrium equation and incremental equilibrium equation of the truss system are acquired from (6), using a finite element formulation to assemble components according to the nodal displacement indices.

$$\begin{aligned} &\boldsymbol{M}\ddot{\boldsymbol{u}} + \boldsymbol{C}\dot{\boldsymbol{u}} + \boldsymbol{q}(\boldsymbol{u}, \Delta_e) = \boldsymbol{P} + \boldsymbol{P}_{imperfect} \\ &\boldsymbol{M}\delta\ddot{\boldsymbol{u}} + \boldsymbol{C}\delta\dot{\boldsymbol{u}} + \boldsymbol{K}(\boldsymbol{u}, \Delta_e)\delta\boldsymbol{u} = \Delta\boldsymbol{P} + \Delta\boldsymbol{P}_{imperfect} \end{aligned} \quad (7)$$

where:

$$\begin{aligned} &\boldsymbol{u} \equiv \{u_1, u_2, ..., u_n\}^T \\ &\delta\boldsymbol{u} \equiv \{\delta u_1, \delta u_2, ..., \delta u_n\}^T \\ &\delta\ddot{\boldsymbol{u}} \equiv \{\delta\ddot{u}_1, \delta\ddot{u}_2, ..., \delta\ddot{u}_n\}^T \\ &\delta\dot{\boldsymbol{u}} \equiv \{\delta\dot{u}_1, \delta\dot{u}_2, ..., \delta\dot{u}_n\}^T \end{aligned} \quad (8)$$

$$\mathbf{M}_{i,j} = \sum_{e=1}^{m} \mathbf{M}_{i,j}^{(e)}; \mathbf{C}_{i,j} = \sum_{e=1}^{m} \mathbf{C}_{i,j}^{(e)}; \quad (9)$$

$$\mathbf{K}_{i,j}(\boldsymbol{u}, \Delta_e) = \sum_{e=1}^{m} \boldsymbol{k}_{i,j}^{(e)}(\boldsymbol{u}, \Delta_e), \ (i, j = 1 \div n) \quad (10)$$

$$\begin{aligned} &\mathbf{q}(\boldsymbol{u}, \Delta_e) \equiv \{\boldsymbol{q}_1(\boldsymbol{u}, \Delta_e), \boldsymbol{q}_2(\boldsymbol{u}, \Delta_e), ..., \boldsymbol{q}_n(\boldsymbol{u}, \Delta_e)\}^T \\ &\mathbf{P} \equiv \{\boldsymbol{P}_1, \boldsymbol{P}_2, ..., \boldsymbol{P}_n\}^T \\ &\Delta\boldsymbol{P} \equiv \{\Delta\boldsymbol{P}_1, \Delta\boldsymbol{P}_2, ..., \Delta\boldsymbol{P}_n\}^T \end{aligned} \quad (11)$$

$$\begin{aligned} &\boldsymbol{q}_i(\boldsymbol{u}, \Delta_e) = \sum_{e=1}^{m} \boldsymbol{q}_i^{(e)}(\boldsymbol{u}, \Delta_e); \boldsymbol{P}_i = \sum_{e=1}^{m} \boldsymbol{P}_i^{(e)}; \\ &\Delta\boldsymbol{P}_i = \sum_{e=1}^{m} \Delta\boldsymbol{P}_i^{(e)}; \boldsymbol{P}_{i,(mperfect)} = \sum_{e=1}^{m} \boldsymbol{P}_{i,(mperfect)}^{(e)}; \\ &\Delta\boldsymbol{P}_{i,(mperfect)} = \sum_{e=1}^{m} \Delta\boldsymbol{P}_{i,(mperfect)}^{(e)}. \end{aligned} \quad (12)$$

The dynamic differential equation is solved by applying the Newmark integration [8, 29]:

$$\begin{cases} \delta\ddot{\boldsymbol{u}} = \dfrac{1}{\beta\Delta t^2}\delta\boldsymbol{u} - \dfrac{1}{\beta\Delta t}\dot{\boldsymbol{u}} - \dfrac{1}{2\beta}\ddot{\boldsymbol{u}} \\ \delta\dot{\boldsymbol{u}} = \dfrac{\gamma}{\beta\Delta t}\delta\boldsymbol{u} - \dfrac{\gamma}{\beta}\dot{\boldsymbol{u}} - \left(\dfrac{\gamma}{2\beta} - 1\right)\Delta t\,\ddot{\boldsymbol{u}} \end{cases} \quad (13)$$

The incremental equilibrium of the truss system displayed in (7) is represented in short form:

$$\bar{\boldsymbol{K}}(\boldsymbol{u}, \Delta_e)\delta\boldsymbol{u} = \Delta\bar{\boldsymbol{P}} \quad (14)$$

where:

$$\begin{aligned} &\bar{\boldsymbol{K}}(\boldsymbol{u}, \Delta_e) = \boldsymbol{K}(\boldsymbol{u}, \Delta_e) + \frac{\boldsymbol{M}}{\beta\Delta t^2} + \frac{\gamma\boldsymbol{C}}{\beta\Delta t} \\ &\Delta\bar{\boldsymbol{P}} = \Delta\boldsymbol{P} + \boldsymbol{M}\left(\frac{1}{\beta\Delta t}\dot{\boldsymbol{u}} + \frac{1}{2\beta}\ddot{\boldsymbol{u}}\right) \\ &\quad + \boldsymbol{C}\left[\frac{\gamma}{\beta}\dot{\boldsymbol{u}} + \left(\frac{\gamma}{2\beta} - 1\right)\Delta t\,\ddot{\boldsymbol{u}}\right] \end{aligned}$$

The Newton–Raphson iterative method is applied to solve the short-form incremental equilibrium equation (14).

III. NUMERICAL EXAMPLE AND DISCUSSION

The investigated planar arch truss, subjected to a step load, consists of *35* elements, as observed in Figure 2. All elements have an elastic modulus of $E = 68.964 \times 10^6$ *kN/m*^{2} [8]. The nodal coordinates of the truss and the cross-sectional areas of the elements are presented in Tables I and II [8, 27, 28]. The nodal mass is $m = 50$ *kg*, and the imperfection loading factor is $e = 0.01$, assuming that only the 1st to the 10th elements have an imperfect length ($\Delta_e^{(1)\div(10)} = 0.381$ *cm*), neglecting damping forces.

This truss has been previously studied in [8] in two separate imperfect cases: (i) a truss subjected to imperfect step loading but with perfect lengths and (ii) a truss with imperfect lengths but subjected to perfect step loading. In the present study, both imperfection factors were considered simultaneously, as displayed in Figure 3. The dynamic equilibrium expressed in (7) contains two types of imperfect parameters, Δ_e, and $\boldsymbol{P}_{imperfect}$, which are solved using the Newton–Raphson algorithm and the Newmark integration method.

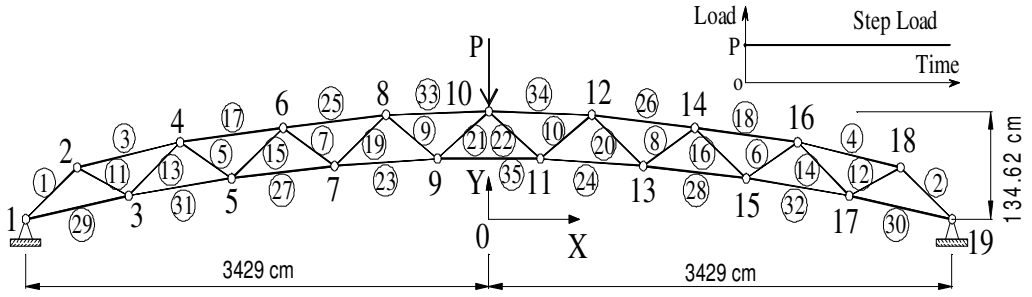

Fig. 2. Arch-truss structure.

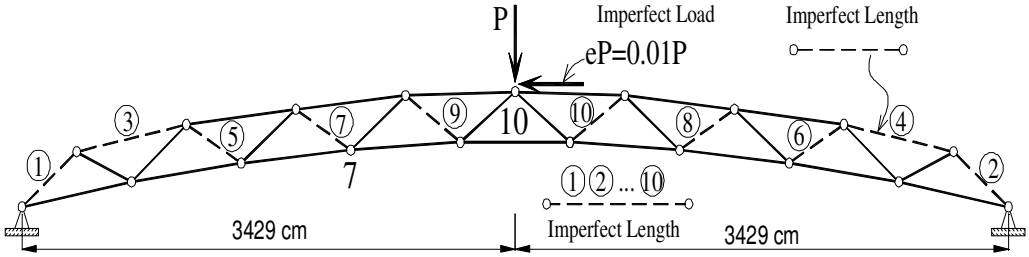

Fig. 3. The arch-truss structure accounting for imperfect length and loading.

TABLE I. COORDINATES OF EACH NODE IN THE ARCH TRUSS

Nodal number	*X* (cm)	*Y* (cm)
19, 1	± 3429.0	0
18, 2	± 3048.0	50.65
17, 3	± 2667.0	34.75
16, 4	± 2286.0	83.82
15, 5	± 1905.0	65.3
14, 6	± 1524.0	110.85
13, 7	± 1143.0	87.99
12, 8	± 762.0	128.5
11, 9	± 381.0	100.65
10	0	134.62

TABLE II. CROSS-SECTIONAL AREAS OF EACH MEMBER IN THE ARCH TRUSS

Member number	Cross-sectional area (cm^2)
1–10, 35	51.61
11, 12	64.52
13–16	83.87
17, 18	96.77
19–22	103.23
23, 24	161.29
25, 26	193.55
27, 28	258.06
29–32	290.32
33, 34	309.68

The calculation results are manifested in Figures 4-6. In Figure 4, the values of the dynamic limit load are provided for the following cases: (i) Perfect System with P_{cr} = 21.68 kN, (ii) Imperfect Loading with P_{cr} = 21.67 kN, (iii) Imperfect Length with P_{cr} = 13.30 kN, and (iv) Imperfect Length and Loading with P_{cr} = 12.72 kN. The dynamic limit load in the case of Imperfect Loading changes insignificantly compared with the Perfect System, suggesting that the influence of imperfect loading is small.

The dynamic limit load in the case of Imperfect Length is 61.3% of the value obtained in the Perfect System. Therefore, the influence of the imperfect length is crucial. When considering both imperfection factors at the same time, the value of the dynamic limit load was 58.6% of that obtained for the Perfect System and 95.6% of that acquired for the Imperfect Length case. Thus, the simultaneous effects of both imperfection factors substantially reduced the dynamic limit load.

Next, the dynamic responses over time were investigated, deploying different load values. The results portrayed in Figures 5 and 6 indicate that the displacement increases rapidly when the load exceeds the dynamic limit load. Specifically, in the Perfect System, when the load $P > P_{cr}$ = 21.68 kN, the displacement increases up to 300 cm. Similarly, in the Imperfect Length and Imperfect Length and Loading cases, the displacement increases rapidly when $P > P_{cr}$ = 13.30 kN and $P > P_{cr}$ = 12.72 kN, respectively.

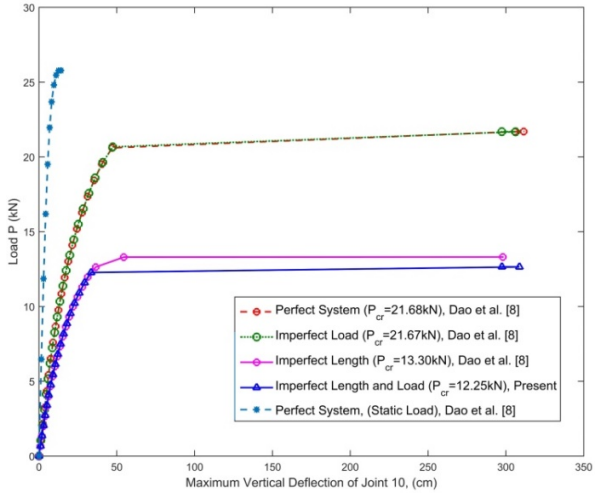

Fig. 4. Maximum vertical displacements at node 10 under step loading.

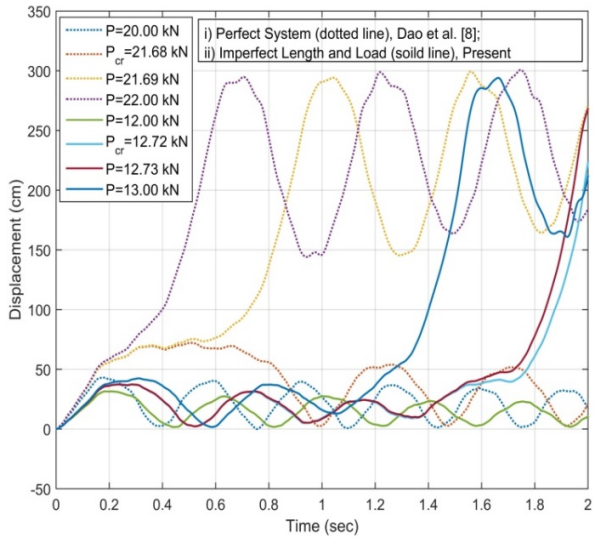

Fig. 5. The vertical displacement of node 10 over time for the perfect system and the case of imperfect length and loading.

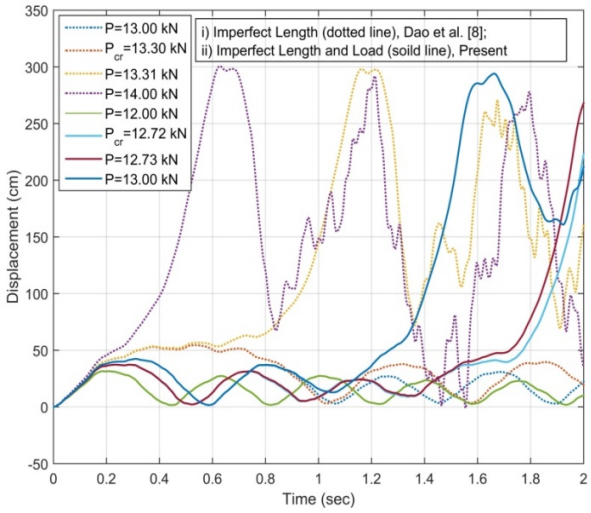

Fig. 6. The vertical displacement of node 10 over time for the imperfect length and the case of imperfect length and loading.

Next, the dynamic responses over time were investigated, deploying different load values. The results portrayed in Figures 5 and 6 indicate that the displacement increases rapidly when the load exceeds the dynamic limit load. Specifically, in the Perfect System, when the load $P > P_{cr} = 21.68$ kN, the displacement increases up to 300 cm. Similarly, in the Imperfect Length and Imperfect Length and Loading cases, the displacement increases rapidly when $P > P_{cr} = 13.30$ kN and $P > P_{cr} = 12.72$ kN, respectively.

IV. CONCLUSIONS

The influence of both the imperfect element length and loading on the dynamic buckling of a planar arch truss was investigated in this paper using a modified hybrid Finite Element Method (FEM). In particular, step loading was considered while accounting for the imperfection factors. The load-maximum displacement relationship, the value of the dynamic limit load, and the transient dynamic responses of the truss corresponding to different cases were established.

The simultaneous influence of the imperfect length and load significantly reduced the value of the limit load although the influence of the imperfect load alone was not crucial. When considering both imperfection factors concurrently, the value of the dynamic limit load decreased to 58.6% of that obtained for the Perfect System. This elucidates the need to simultaneously contemplate both the imperfect element length and load factors when studying the dynamic buckling of truss systems.

REFERENCES

[1] D. T. Thuy, L. N. Ngoc, D. N. Tien, and H. V. Thanh, "An Analytical Solution for the Dynamics of a Functionally Graded Plate resting on Viscoelastic Foundation," *Engineering, Technology & Applied Science Research*, vol. 13, no. 1, pp. 9926–9931, Feb. 2023, https://doi.org/10.48084/etasr.5420.

[2] T. T. Nguyen, "Influence of Material and Geometry Defects on Local Buckling Resistance of FRP Columns," *Transport and Communications Science Journal*, vol. 74, no. 5, pp. 611–626, 2023, https://doi.org/10.47869/tcsj.74.5.54.

[3] P. C. Nguyen, B. Le-Van, and S. D. T. V. Thanh, "Nonlinear Inelastic Analysis of 2D Steel Frames : An Improvement of the Plastic Hinge Method," *Engineering, Technology & Applied Science Research*, vol. 10, no. 4, pp. 5974–5978, Aug. 2020, https://doi.org/10.48084/etasr.3600.

[4] P. C. Nguyen, "Nonlinear Inelastic Earthquake Analysis of 2D Steel Frames," *Engineering, Technology & Applied Science Research*, vol. 10, no. 6, pp. 6393–6398, Dec. 2020, https://doi.org/10.48084/etasr.3855.

[5] N. C. T. Thanh, "Analytical truss model for concrete beams reinforced with FRP bars," *Transport and Communications Science Journal*, vol. 74, pp. 456–468, May 2023, https://doi.org/10.47869/tcsj.74.4.6.

[6] H. T. Duy, N. D. Diem, G. V. Tan, V. V. Hiep, and N. V. Thuan, "Stochastic Higher-order Finite Element Model for the Free Vibration of a Continuous Beam resting on Elastic Support with Uncertain Elastic Modulus," *Engineering, Technology & Applied Science Research*, vol. 13, no. 1, pp. 9985–9990, Feb. 2023, https://doi.org/10.48084/etasr.5456.

[7] D. H. Duc, D. V. Thom, and P. M. Phuc, "Buckling Analysis of Variable Thickness Cracked Nanoplates Considering the Flexoelectric Effect," *Transport and Communications Science Journal*, vol. 73, no. 5, pp. 470–485, 2022, https://doi.org/10.47869/tcsj.73.5.3.

[8] N. T. Dao and T. V. T. Thi, "Hybrid Finite Element Method in Nonlinear Dynamic Analysis of Trusses," *International Journal of Structural Stability and Dynamics*, vol. 23, no. 20, Dec. 2023, Art. no. 2450195, https://doi.org/10.1142/S0219455424501955.

[9] J. P. Pascon, "Nonlinear analysis of hyperelastoplastic truss-like structures," *Archive of Applied Mechanics*, vol. 86, no. 5, pp. 831–851, May 2016, https://doi.org/10.1007/s00419-015-1065-9.

[10] E. Murtha-Smith, "Nonlinear Analysis of Space Trusses," *Journal of Structural Engineering*, vol. 120, no. 9, pp. 2717–2736, Sep. 1994, https://doi.org/10.1061/(ASCE)0733-9445(1994)120:9(2717).

[11] A. K. Noor, "Nonlinear Analysis of Space Trusses," *Journal of the Structural Division*, vol. 100, no. 3, pp. 533–546, Mar. 1974, https://doi.org/10.1061/JSDEAG.0003737.

[12] M. Greco and C. E. R. Vicente, "Analytical solutions for geometrically nonlinear trusses," *Rem: Revista Escola de Minas*, vol. 62, no. 2, pp. 205–214, Jun. 2009, https://doi.org/10.1590/S0370-44672009000200012.

[13] C. Cichon and L. Corradi, "Large displacement analysis of elastic-plastic trusses with unstable bars," *Engineering Structures*, vol. 3, no. 4, pp. 210–218, Oct. 1981, https://doi.org/10.1016/0141-0296(81)90003-1.

[14] H.-T. Thai and S.-E. Kim, "Large deflection inelastic analysis of space trusses using generalized displacement control method," *Journal of Constructional Steel Research*, vol. 65, no. 10, pp. 1987–1994, Oct. 2009, https://doi.org/10.1016/j.jcsr.2009.06.012.

[15] J. A. T. de Freitas and A. C. B. S. Ribeiro, "Large displacement elastoplastic analysis of space trusses," *Computers & Structures*, vol. 44, no. 5, pp. 1007–1016, Aug. 1992, https://doi.org/10.1016/0045-7949(92)90323-R.

[16] S. S. Ligarò and P. S. Valvo, "Large displacement analysis of elastic pyramidal trusses," *International Journal of Solids and Structures*, vol. 43, no. 16, pp. 4867–4887, Aug. 2006, https://doi.org/10.1016/j.ijsolstr.2005.06.100.

[17] A. El-Sheikh, "Approximate dynamic analysis of space trusses," *Engineering Structures*, vol. 22, no. 1, pp. 26–38, Jan. 2000, https://doi.org/10.1016/S0141-0296(98)00075-3.

[18] D. R. Sherman, "Latticed Structures: State-of-the-Art Report," *Journal of the Structural Division*, vol. 102, no. 11, pp. 2197–2230, Nov. 1976, https://doi.org/10.1061/JSDEAG.0004479.

[19] S. M. Holzer, W. S. White, A. E. Somers, and R. H. Plaut, "Stability of Lattice Structures Under Combined Loads," *Journal of the Engineering Mechanics Division*, vol. 106, no. 2, pp. 289–305, Apr. 1980, https://doi.org/10.1061/JMCEA3.0002585.

[20] A. Y. T. Leung, H. X. Yang, and P. Zhu, "Nonlinear Vibrations of Viscoelastic Plane Truss Under Harmonic Excitation," *International Journal of Structural Stability and Dynamics*, vol. 14, no. 04, May 2014, Art. no. 1450009, https://doi.org/10.1142/S0219455414500096.

[21] Y. L. Guennec, É. Savin, and D. Clouteau, "A time-reversal process for beam trusses subjected to impulse loads," *Journal of Physics:*

Conference Series, vol. 464, no. 1, Oct. 2013, Art. no. 012001, https://doi.org/10.1088/1742-6596/464/1/012001.

[22] A. Kassimali and E. Bidhendi, "Stability of trusses under dynamic loads," *Computers & Structures*, vol. 29, no. 3, pp. 381–392, Jan. 1988, https://doi.org/10.1016/0045-7949(88)90391-4.

[23] K. Zhu, F. G. A. Al-Bermani, and S. Kitipornchai, "Nonlinear dynamic analysis of lattice structures," *Computers & Structures*, vol. 52, no. 1, pp. 9–15, Jul. 1994, https://doi.org/10.1016/0045-7949(94)90250-X.

[24] C.-Y. Wang, R. Wang, C.-C. Chuang, and T.-R. Wu, "Nonlinear Dynamic Analysis of Reticulated Space Truss Structures," *Journal of Mechanics*, vol. 22, pp. 199–212, Sep. 2006, https://doi.org/10.1017/S1727719100000848.

[25] G. Liu, G. Chen, and F. Cui, "Nonlinear dynamic analysis of ring truss antenna equivalent to the cylindrical shell with thermal excitation," *European Journal of Mechanics - A/Solids*, vol. 85, Jan. 2021, Art. no. 104109, https://doi.org/10.1016/j.euromechsol.2020.104109.

[26] B. Budiansky and J. W. Hutchinson, "Dynamic buckling of imperfection-sensitive structures," in *Applied Mechanics*, Berlin, Heidelberg, Germany: Springer, 1966, pp. 636–651, https://doi.org/10.1007/978-3-662-29364-5_85.

[27] K. Kondoh and S. N. Atluri, "Influence of local buckling on global instability: Simplified, large deformation, post-buckling analyses of plane trusses," *Computers & Structures*, vol. 21, no. 4, pp. 613–627, Jan. 1985, https://doi.org/10.1016/0045-7949(85)90140-3.

[28] M. A. M. Torkamani and J.-H. Shieh, "Higher-order stiffness matrices in nonlinear finite element analysis of plane truss structures," *Engineering Structures*, vol. 33, no. 12, pp. 3516–3526, Dec. 2011, https://doi.org/10.1016/j.engstruct.2011.07.015.

[29] A. K. Chopra, Dynamics of Structures: Theory and Applications to Earthquake Engineering, 2nd ed. Upper Saddle River, NJ, USA: Prentice Hall, 2000.

[30] K.-J. Bathe, *Finite Element Procedures*, 2nd ed. Watertown, MA, USA: Klaus-Jürgen Bathe, 2014.